Degradation of hydroxycinnamic acid mixtures in aqueous sucrose solutions by the Fenton process

Danny M.T. Nguyen,[†] Zhanying Zhang,[‡] and William O.S. Doherty,*[,†]

[†] Sugar Research and Innovation, Centre for Tropical Crops and Biocommodities,

[‡] Centre for Tropical Crops and Biocommodities, Queensland University of Technology, Brisbane, QLD 4000, Australia

* Corresponding author

Contact:

Email: w.doherty@qut.edu.au

Postal address: GPO Box 2432, 2 George St, Brisbane, QLD 4001, Australia

ABSTRACT: The degradation efficiencies and behaviors of caffeic acid (CaA), *p*-coumaric acid (*p*CoA) and ferulic acid (FeA) in aqueous sucrose solutions containing the mixture of these hydroxycinnamic acids (HCAs) mixtures were studied by the Fenton oxidation process. Central composite design and multi-response surface methodology were used to evaluate and optimize the interactive effects of process parameters. Four quadratic polynomial models were developed for the degradation of each individual acid in the mixture and the total HCAs degraded. Sucrose was the most influential parameter that significantly affected the total amount of HCA degraded. Under the conditions studied there was < 0.01% loss of sucrose in all reactions. The optimal values of the process parameters for a 200 mg/L HCA mixture in water (pH 4.73, 25.15 °C) and sucrose solution (13 mass%, pH 5.39, 35.98 °C) were 77% and 57% respectively. Regression analysis showed goodness of fit between the experimental results and the predicted values. The degradation behavior of CaA differed from those of *p*CoA and FeA, where further CaA degradation is observed at increasing sucrose and decreasing solution pH. The differences (established using UV/Vis and ATR-FTIR spectroscopy) were because, unlike the other acids, CaA formed a complex with Fe(III) or with Fe(III) hydrogen-bonded to sucrose, and coprecipitated with lepidocrocite, an iron oxyhydroxide.

KEYWORDS: advanced oxidation process; color precursor; sucrose, sugar juice; Fenton; hydroxycinnamic acid

INTRODUCTION

The food industry is concerned with progressive decay and color formation of fresh and processed food largely due to the oxidation of phenolic compounds in the presence of carbohydrates and proteins (*1*). Research on understanding the formation and degradation of these compounds is receiving significant attention. In the sugar industry, reducing raw sugar color not only reduces refinery costs but also improves its nutrition potential.

A number of methods including adsorption and oxidation have been developed to remove phenolic compounds from either wastewater or food products. Advanced oxidation processes (AOPs) have shown promising effects on remove phenolic compounds. The basic process is the Fenton process, and it involves the reaction of Fe(II) and H_2O_2 at a typical pH of 2.8. The radicals formed breakdown the phenolic compounds. In the last decade, much attention has been paid to the variations and development of Fenton reaction-based AOPs to improve the oxidation performance and alleviate one of the major drawbacks of the Fenton process, namely the production of iron sludge. These include photo-Fenton (*e.g.*, solar and UV) (*2, 3*), electro-Fenton (*4*), sono-Fenton (*5*), Fenton-like (*e.g.*, Fe(III), chelated iron) (*6, 7*) and heterogeneous Fenton (*e.g.*, Fe-pillared clays, zero valent iron (ZVI)) (*8, 9*). However, most of these technologies have not yet been commercialized because of issues surrounding operating costs. Therefore, the conventional Fenton process, which is simple and requires no specialized equipment, is still the only cost-effective process to treat a wide range of compounds and convert them into less harmful compounds that are easier to be removed through other purification techniques (*i.e.*, filtration, coagulation, ion-exchange) (*10-12*).

Three hydroxycinnamic acids (HCAs) (*i.e.*, caffeic acid (CaA), *p*-coumaric acid (*p*CoA) and ferulic acid (FeA)) are the three commonly used as phenolic model compounds to mimic color precursors present in food and effluent discharged during food processing (*e.g.*, sugar manufacture). These phenolic acids generally exist in a free, esterified or glycosylated form in plants and under the harsh conditions that prevail during food processing, these esterified or glycosylated phenolic acids break down to free phenolics (*13, 14*). The degradation of mixtures of phenolic compounds has been studied using Fenton oxidation (*15*), Fenton-like oxidation (*16*), ozone (*17*) and other AOPs (mainly photocatalysis processes) (*18-21*). Heredia et al., (*15*) developed a kinetic model for the oxidation of phenolic compounds (including CaA, *p*CoA and FeA) by the Fenton process. The rate constants for the degradation of the individual phenolic acids in a mixture of acids, were deduced from the developed model and it was found that the degradation process at a constant Fe(II) concentration at 30 °C proceeded in the following order FeA > *p*CoA > CaA. No reason was given for the differences in the rate of degradation among these HCA mixtures. None of these studies optimized the degradation process of individual acids within a mixture of phenolic acids by the Fenton process, nor examined the interactive effects of various operating parameters on the degradation of each acid. Also, the role of sucrose (apart from its free radical scavenging ability) in the degradation process of these acids in a mixture has not been reported (*22*).

CaA, *p*CoA and FeA are also the main color precursors present in sugar cane juice and are known to participate in reactions producing color that results in the raw sugar (sucrose) product (*23, 24*). In this study, a comprehensive investigation on the degradation of CaA, *p*CoA and FeA in aqueous sucrose solutions containing the mixture of these HCAs was conducted. The degradation efficiencies and behaviors of

individual HCAs were studied. The degradation conditions were optimized using central composite design (CCD) and multi-response surface methodology (MRSM). Models were developed to predict the degradation of HCA mixtures in synthetic sugar cane juice solutions and examined by regression analysis.

MATERIALS AND METHODS

Reagents and solvents

CaA, *p*CoA, FeA; fructose, glucose, lactose and sucrose were obtained from Sigma-Aldrich (St. Louis, MO, USA). Ferrous sulphate heptahydrate ($FeSO_4 \cdot 7H_2O$), glacial acetic acid, hydrogen peroxide (H_2O_2, 30% w/w), sodium acetate, sodium hydroxide and sulphuric acid were purchased from APS Ajax Finechem (Seven Hills, NSW, Australia). Ethanol (absolute) was supplied from Merck (Darmstadt, Germany). All chemicals were purchased of the highest purity grade available and used as supplied without any further purification. Stock solutions of hydroxycinnamic acids, HCAs (*i.e.*, CaA, *p*CoA and FeA, 10 mg/mL) were prepared individually by dissolution in degassed aqueous ethanol solution (50% v/v) and stored at 4.0 °C in the absence of UV light.

Fenton oxidation reactions

Reactions were carried out in 10 mL glass scintillated reaction vessels housed in an Pierce Reacti-Therm heating/stirring module (Rockford, IL, USA) with continuous magnetic stirring (280 rpm). In each run, a predetermined amount of high purity water (18.2 MΩ·cm), sucrose and each HCA were added to the reaction vessel. A consistent amount of $FeSO_4 \cdot 7H_2O$ and H_2O_2 solutions were added to achieve a final volume of 5.0 mL and a final concentration of 0.5 mM and 7.50 mM, respectively.

94 The optimum working molar ratio (Fe(II)/H_2O_2) determined for the Fenton reaction
95 by the authors was 1:15 (*25*). The reaction was initiated as soon as H_2O_2 was added.
96 After 2 min, 3 mL of the solution was taken, diluted 10-fold to quench the reaction
97 and kept frozen. Table 1 gives the operating conditions used in the Fenton oxidation
98 process. The reaction time was kept to 2 min in order to minimize sucrose degradation
99 in order to allow treatment of sugar cane process streams, where the main objective is
100 to preserve the sucrose content.

101 Although it is well known that ethanol is a scavenger for hydroxyl radical, in this
102 study, ethanol had to be used for the dissolution of HCAs due to the low solubility of
103 HCAs in water. As the ethanol concentration was at least 11 times higher than the
104 concentrations of Fe (II) and H_2O_2 (0.5 mM and 7.5 mM respectively), it was
105 assumed that the effect of ethanol on the Fenton reaction was similar.

106 **Instrumental procedures and analyses**

107 The proportion of each HCA degraded was monitored by reversed-phase HPLC with
108 UV-visible (UV/Vis) diode-array detection (DAD). The analysis was performed on a
109 Hewlett Packard HP/Agilent 1100 Series HPLC system (Germany) using a Waters
110 Symmetry C18 column (150 mm length × 3.9 mm diameter) with a Waters Guard-Pak
111 Resolve C18 guard insert (10 μm) (Milford, MA, USA). The mobile phase consisted
112 of 1.0% v/v acetic acid in water (as eluent A) and methanol (as eluent B). The
113 gradient program was as follows: 20% B to 25% B (5 min), 25% B to 50% B (15 min)
114 and 50% B to 20% B (5 min). Simultaneous detection at specific wavelengths (280
115 nm and 320 nm) subtracted against a reference wavelength (620 nm). The column
116 temperature was ambient (25 °C) and the flow rate of mobile phase was 1.0 mL/min.
117 Aliquots of samples were membrane filtered (0.45 μm) prior to injection into the

HPLC system. Sucrose and reducing sugar contents in the reaction mixtures were monitored by a Waters HPLC system with (Milford, MA, USA) equipped with a 626 pump, a 600S controller, a 717plus autosampler and a 2465 electrochemical detector. A Dionex CarboPac PA-1 anion exchange column (250 mm × 4 mm) with a Dionex CarboPac PA-1 guard column (50 mm length × 4 mm diameter) (Waltham, MA, USA) was used to separate the sugars at 27 °C with 150 mM sodium hydroxide as mobile phase (a flow rate of 1.0 mL/min). The samples were diluted 100 times and filtered through 0.45 μm membrane disc filters prior to HPLC analysis.

The efficiency of the Fenton process on the degradation of CaA, *p*CoA and FeA was determined individually based on the change in absorbance of the corresponding HPLC peak, using Eq. (1):

$$\%\ \text{CaA, } p\text{CoA or FeA degradation} = \left(\frac{A_0 - A_t}{A_0}\right) \times 100 \quad (1)$$

where A_0 is initial absorbance of HCA in mAU (*i.e.*, $t = 0$ min) and A_t is absorbance of HCA in mAU at time of aliquot taken (*i.e.*, $t = 2$ min)

Experimental design and statistical analysis

Design of experiments, mathematical modelling and optimization of process parameters were evaluated using the Stat-Ease Inc. Design-Expert 7.0.0 software package (Minneapolis, MN, USA). A rotatable circumscribed central composite design (CCD) was used to evaluate the main effect for each condition and the possible interactive effects on the residual stresses between two variables. The process parameters (independent variables) used in this study are the initial total HCA concentration (*A*), the initial sucrose concentration (*B*), the solution pH (*C*), and the

reaction temperature (*D*). The selected response factors (dependent variables) for optimization are % CaA degradation (y_1), % *p*CoA degradation (y_2), % FeA degradation (y_3) and % total HCA degradation (y_4). The coded and actual values of each variable and their levels for the experimental design used in the study are shown in Table 1. The ranges for each parameter were determined by preliminary experiments based on previous work by the authors (*23*) and were selected to closely mimic operating parameters during the processing of sugar cane juice for raw sugar manufacture. Concentrations of HCAs varied from 20–200 mg/L to mimic the range of HCAs and phenolic compounds concentrations in sugar cane juice, which depends on season, region and type of cane and the method of harvesting (*e.g.*, burnt cane, green cane, whole crop cane).

Analysis of variance (ANOVA) was used for model adequacy and analysis of the experimental data. The quality of the fit polynomial model was expressed by the regression coefficient, R^2 and its statistical significance was checked using Fisher's F-test.

Evaluation of the interactions between Fe(II) and HCAs

Studies were conducted to investigate the interaction between Fe(II) and each of the HCAs in the presence and absence of sucrose using UV/Vis and attenuated total reflectance-Fourier transform infrared (ATR-FTIR) spectroscopy. Sodium acetate (100 mM) and acetic acid (100 mM) solutions were used to make buffer solutions having pH values of 4.0 to 6.0. For each analysis, a predetermined amount of buffer, sucrose and $FeSO_4.7H_2O$ were added to achieve a final HCA concentration of 5.50 mM. Samples were diluted to the desired concentration and immediately membrane disc filtered (0.45 μm) for analysis. The pH of each solution was checked before and

after dilution. The UV/Vis spectra were recorded on a Perkin Elmer Lambda 35 double-beam UV-visible spectrophotometer (Shelton, CT, USA) using cells of 1.0 cm path length and at a wavelength range of 190–450 nm in 1.0 nm increments. Data acquisition was performed using the Perkin Elmer UV WinLab (Ver. 2.85.04) software package.

Infrared absorbance spectra were obtained using a Thermo Electron Nicolet Nexus 870 FT-IR instrument fitted with a deuterated triglycine sulphate (DTGS) detector (Madison, WI, USA). Spectra were recorded over the 4000–650 cm^{-1} range at 4 cm^{-1} resolution for 64 scans with an optical path difference (OPD) velocity of 0.6329 cm/s. Data acquisition and processing was performed using the OMNIC 7.3 software package. The FTIR peaks were normalized with respect to the main peak at 1045 cm^{-1}.

A light brown precipitate was formed at pH $\geq$ 5 for all the acids with iron. No recoverable amount precipitate was obtained at lower pH. This precipitate was filtered using a polyvinyl chloride (PVC) membrane filter (5 μm) and the retentate was analyzed by X-ray powder diffraction (XRD). Sample analysis was performed on a PANalytical X'Pert PRO multi-purpose X-ray diffractometer (MPD) (Almelo, Netherlands) using Cu Kα radiation (λ = 1.5406 Å) at 40 kV and 40 mA. Patterns were recorded in the 2θ range from 3.5° to 75° with a scan step size of 0.017° and a count time per step of 50 s. Data was acquired and processed using the X'Pert Data Collector 2.2 and MDI Jade 9.0 software packages respectively.

RESULTS AND DISCUSSION

Optimal data transformation and test for normality

186 CCD and response surface methodology (RSM) were used to investigate the
187 relationships between the response factors (dependent variables) and the process
188 parameters (independent variables). In order to achieve this, an empirical second-
189 order polynomial function for each response investigated with respect to the four
190 process parameters was used to fit the experimental results obtained, as described by
191 (*26*).

192 A normal probability plot of residuals based on the experimental data obtained for
193 CaA degradation (Figure 1) indicates a non-linear pattern in the middle of the trend
194 line, and short tails with the first and last few points showing increasing departure
195 from the trend line. To address the non-linearity of these plots, the Box-Cox power
196 transformation was used to improve linearity. The power transformation on the
197 predicted response can be described as follows (*27*):

$$y^{(\lambda)} = \begin{cases} \dfrac{y^{\lambda} - 1}{\lambda} & \lambda \neq 0 \\ \ln(y) & \lambda = 0 \end{cases} \qquad (2)$$

198 where λ indicates the power to which all data should be raised. The initial value of λ
199 in the standard quadratic function (*i.e.*, Eq. (2)) is $\lambda = 1.00$.

200 To determine the λ value for each response, a Box-Cox plot was used as a guide for
201 the selection of the optimized λ value for the power transformation of the
202 experimental data. Supplementary Figure 1 shows the Box-Cox plots for each
203 response investigated. From the Box-Cox plots for the *p*CoA (Supplementary Figure
204 1b) and FeA (Supplementary Figure 1c) degradation data, the recommended λ values
205 ranged from 0.70 to 2.40 and 0.59 to 2.23, respectively at a 95% confidence interval.
206 On the other hand, the λ value range within the 95% confidence interval were not

shown for CaA (Supplementary Figure 1) and total HCA (Supplementary Figure 1d) degradation data, due to the values being outside the $\lambda = \pm 3.00$ limits. Hence, the optimum λ values used to transform the CaA and total HCA degradation were both maximized at $\lambda = 3.00$. For *p*CoA and FeA degradation, the optimum λ values were determined by observing the minimum of the curve, which was 1.56 and 1.43 respectively. Using the optimized λ values, the normal probability plot for each response surface model shown in Supplementary Figure 2 indicate improved linearity of data points. There are only a minimal number of data points deviating from the line of fit. The data for all fitted response surface models show good correspondence to a normal distribution and validated the normality assumption.

Regression modelling and statistical analysis

On the basis of the sequential model sum of squares (Type I), the power transformed response surface models for CaA (y_1), *p*CoA (y_2), FeA (y_3) and total HCA (y_4) degradation were selected based on the highest order polynomial, where the additional model terms were significant and the models were not aliased. The data obtained for all four responses fit a quadratic polynomial function.

The ANOVA results for the partial sum of squares (Type III) for the four response surface reduced quadratic models after stepwise regression are shown in Supplementary Table 1. The analysis indicates that most independent variables and some of the interactions are significant and contribute to the degradation of the HCAs. Model terms with a *p*–value < 0.0500 indicate model terms are significant at the 95% confidence level. Values > 0.1000 indicate the model terms are insignificant at the 90% confidence level and are removed from the proposed models via stepwise regression, with the exception of the first-order temperature model term for all models.

231 Temperature was regarded as statistically insignificant but was added to all models to
232 make each model hierarchical. In other words, parent (*i.e.*, first-order) model terms
233 are added to the model to complete the family of any significant higher-order (*i.e.*,
234 second-order) model terms.

235 The independent variables in the models were initial total HCA concentration, initial
236 sucrose concentration, solution pH and reaction temperature; and were coded A, B, C
237 and D respectively. The final empirical quadratic equations in terms of coded factors
238 for each response are as follows:

CaA degradation (%)

$$(y_1)^3 = 7.459 \times 10^5 - 22685.04A + 87649.64B - 1.893 \times 10^5 C - 2787.88D + 38875.43BC + 25613.66BD - 48866.47B^2 - 55229.82C^2 + 21771.66D^2 \quad (3)$$

pCoA degradation (%)

$$(y_2)^{1.56} = 452.03 - 25.39A - 112.96B + 56.46C - 9.29D + 25.34AB + 24.11CD + 51.51B^2 - 13.11C^2 \quad (4)$$

FeA degradation (%)

$$(y_3)^{1.43} = 274.79 - 14.82A - 69.60B + 25.99C - 3.36D + 24.97AB - 9.36BD + 6.34\,CD + 26.42B^2 + 9.46D^2 \quad (5)$$

Total HCA degradation (%)

$$(y_4)^3 = 2.670 \times 10^5 - 22911.69A - 49869.11B - 10752.76C - 4168.93D + 19018.79AB + 17344.68BC + 14113.81CD + 9351.73B^2 - 19861.54C^2 + 11289.82D^2 \quad (6)$$

239 The predicted R^2 values of all response surface models are in reasonable agreement
240 with the adjusted R^2 values, which show that the fitted models are adequate. The

241 accuracy of the models is shown in Figure 2, which compares the predicted responses
242 against the experimental data. Reasonable linear relationships were obtained for
243 predicting the degradation of *p*CoA and FeA (Figure 2b & 2c) but not for *CaA* and
244 total HCAs (Figure 2a and 2d), respectively. This may be related to complex
245 formation as discussed in section 3.4.

246 On the basis of the coefficients of the first-order model terms in Eqs. (3–6), it is
247 evident that the degradation efficiency of all HCAs decreases with the increase of the
248 initial total HCA concentration (*A*). Sucrose concentration (*B*) is the most influential
249 parameter with the highest coefficient in all equations and shows a negative influence
250 in *p*CoA and FeA degradation but a positive influence for CaA degradation. Also, the
251 degradation efficiency of *p*CoA and FeA increases with solution pH (*C*) but the
252 opposite is observed for CaA (refer to the section on complex formation).
253 Temperature (*D*) has a negative effect on all responses but its minuscule coefficient
254 has little effect on the respective response. Hence, this model term is statistically
255 insignificant and was only included in all of the equations to make the models
256 hierarchical.

257 For the degradation of the mixture (*i.e.*, the combined acids), there are strong
258 interactions between total HCA concentration and sucrose (*AB*), between sucrose and
259 pH (*BC*), and between pH and temperature (*CD*).

260 **Perturbation analysis**

261 Perturbation plots were analyzed in order to further identify the most influential
262 variables on the degradation of each HCAs investigated in this study (Figure 3).
263 Sucrose concentration and solution pH appeared to be the most influential parameters.

264 Temperature showed an insignificant effect as expected, whilst the initial total HCA
265 concentration exhibited a consistent effect for the degradation of each HCA.

266 As shown in Figure 3a–c, the higher the initial total HCA concentration, the lower the
267 amount of each HCA degraded. The reason behind the decrease in degradation
268 efficiency is simply due to a higher uptake of •OH radicals by the increased amounts
269 of HCA molecules.

270 The presence of sucrose significantly affected the degradation efficiency of the HCAs.
271 The fate of sucrose during the degradation process was evaluated by HPAEC-PAD.
272 The results showed up to 0.01% sucrose loss due to complete mineralization, as no
273 glucose and/or fructose are detected. This is related to the effective scavenging ability
274 of sucrose in removing •OH radicals (*22*), and accounts for the decrease in
275 degradation efficiency with increasing in sucrose concentration for *p*CoA and FeA
276 (Figure 3b and 3c), but not for CaA (Figure 3a). The reason for the increased
277 degradation efficiency of CaA with increasing sucrose concentration, may be related
278 as will be shown in the next section, to a strong association between CaA and sucrose
279 which increased with increasing sucrose concentration, and precipitation of CaA out
280 of solution.

281 Degradation of CaA decreases with increasing pH whereas the opposite was observed
282 for *p*CoA and FeA degradation. The reason for the results obtained with *p*CoA and
283 FeA is not known but may be related to the various species that exist in the acid-base
284 equilibria that influences the logarithmic acid dissociation constants (pK_a's) of these
285 acids. The results obtained with CaA, with increasing pH are again related to the
286 precipitation of the latter as shown later.

Complex formation

In order to obtain insights into the apparent differences in the behavior among the three HCAs, the UV/Vis spectra of the individual acids, mixtures of each acid with Fe(II) and mixtures of each acid with Fe(II) and sucrose at pH 4.0 to 6.0 were obtained. The UV/Vis spectra obtained with mixtures of FeA or mixtures of *p*CoA were not dissimilar to that of their corresponding acids. However, as Figure 4 shows, there is a significant difference between the spectra of CaA with Fe(II) and those spectra without Fe(II). In these acidic conditions, Fe(II) and Fe(III) will be present in equilibrium (*28*). The change in the profile of the spectra is likely due to complexation between Fe(III) and CaA, as shown in the spectra obtained for Al(III)-CaA in aqueous acidic solutions by Cornard and co-workers (*29*). In fact, Hynes and O'Coinceanainn (*30*) have reported the formation of 1:1 complex between Fe(III) and CaA at pH between 1 and 2.5 (Scheme 1). Moreover, previous studies have shown the accelerated decomposition of H_2O_2 to •OH radicals by Fe(III) complexes of analogous phenolic acids (*31*).

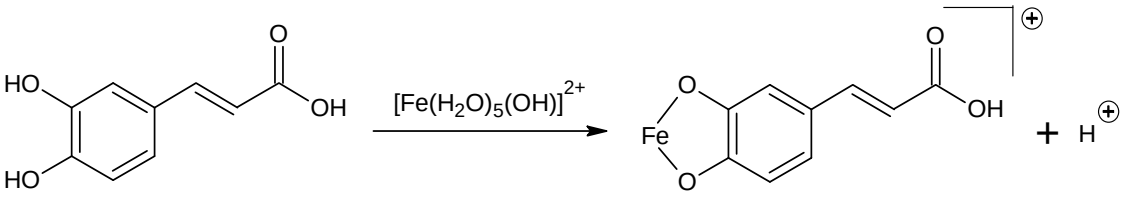

Scheme 1

There is a shape drop in peak intensities at pH ≥ 5 for CaA and Fe(III) mixtures (Figure 4b), likely to be associated with increased complex formation due to increasing amounts of caffeate ions with pH rise. As the pK_{a1} of CaA is 4.38, there is an increasing amount of deprotonation with increasing pH (*32*). The drop in intensity may also be due to the removal of CaA by adsorbing onto the iron precipitate formed

309 under these pH conditions. The spectra of Figure 4b also show that there was no
310 change in the shape of the curves with increasing pH, so it is probable that only one
311 type of complex is formed between Fe(III) and CaA under the conditions investigated.

312 The CaA mixtures were further characterized using ATR-FTIR spectroscopy. From
313 the FTIR data, a number of bands were used to monitor changes in CaA as a result of
314 the presence of Fe(II), and the presence of Fe(II) and sucrose. The spectral bands of
315 CaA and sucrose solutions, and CaA mixtures containing Fe(II) or Fe(II) and sucrose
316 are given in Table 2. Spectral bands were assigned based on literature data for CaA
317 (*33-36*), similar phenolic acids (*37-40*) and sucrose (*41-45*). Bands attributable to
318 aromatic ring vibrations are numbered using the Wilson notation adapted by Varsányi
319 (*46*). The main differences between the spectrum of CaA and that of Fe(II)–CaA are
320 shown in Figure 5. The $\nu(CC)_{ar}$ aromatic bands (*i.e.*, 8a and 19a) that occur at 1554
321 cm^{-1} and 1483 cm^{-1} (*36*) are of increased intensity in the Fe(II)–CaA mixture than
322 that of CaA (Figure 5). The peak at ~1386 cm^{-1} associated with $\nu(CC) + \beta(OH)_{ar}$ (*i.e.*,
323 14) (*36*) is also of higher intensity in the spectrum containing both Fe(II) and CaA.
324 These increases in intensity may be attributed to complex formation between the
325 aromatic –OH group in CaA and Fe (III) (*39*). The peak at 1275 cm^{-1} attributable to
326 ν(C–OH) for CaA (*35, 47*) has shifted to a lower wavelength of 1265 cm^{-1} with
327 increase in intensity. This is a further confirmation of a strong association between
328 Fe(III) and CaA and that the complex formed is between Fe(III) and the phenolic
329 hydroxyl group (*30, 31*). There was no change in the band at 1672 cm^{-1} associated
330 with ν(C=O) implying no evidence of Fe (III) bonding to the carboxylic acid group of
331 CaA. Previous works have shown that with other phenolic acids, linkages are formed
332 with their carboxylic acid groups (*37-39*).

333 The spectrum for CaA, Fe (II) and sucrose (Figure 6) show that the broad band that
334 occurs at 3495 cm^{-1} ν(OH) (*45*) which is associated with sucrose has shifted by 94
335 cm^{-1} to a lower wavenumber of 3401 cm^{-1}. This implies hydrogen-bonding
336 interactions between CaA, Fe(III) and sucrose and could well explain why CaA
337 degradation increases with increasing sucrose concentration (*48*). These interactions
338 provide supporting evidence of the differences in the degradation behavior of CaA
339 and the other two HCAs (*viz.*, *p*CoA and FeA). It is also probable that the complex
340 formation between sucrose-Fe(III)-CaA may result in the co-precipitation of CaA,
341 causing its reduction in the system, and not due to its oxidation. As reported in the
342 next section, XRD data showed the co-precipitation of CaA.

343 **Response surface analysis**

344 Graphical representations of the regression model in the form of three-dimensional
345 surface plots were used to provide a pictorial view of the interactions between the
346 independent variables on total HCA degradation. These plots are shown in Figure 7,
347 where two independent variables were varied within the experimental ranges
348 investigated while the remaining variables were kept constant. The interactions are
349 significant as the curvature of the surfaces is obvious.

350 The variables of sucrose concentration and initial total HCA concentration were
351 varied as shown in Figure 7a, whilst the other variables, namely pH and temperature
352 were kept constant at 5.0 and 35 °C respectively. These fixed values were chosen as
353 they were similar to that typical of process sugar cane juice (*23*). The total HCA
354 degradation efficiency decreases with increasing sucrose concentration and the initial
355 total HCA concentration. Increasing the initial total HCA concentration did not
356 significantly decrease the degradation efficiency of the HCAs. This can be seen by

357 both the coefficient of the first- and second-order model term (Eq. (6)) for total HCA
358 concentration (*i.e.*, *A*) and in Figure 7a where there was only a 5.9% discrepancy
359 between 65 and 155 mg/L of initial total HCA at 3.75 mass% sucrose. This
360 discrepancy is not noticeable at higher sucrose concentrations. It can be said from
361 these observations, that the optimal Fenton dosage is capable of degrading higher
362 concentrations of HCAs and other components (similar to that of HCAs) than at the
363 highest concentration studied (*i.e.*, > 200 mg/L).

364 Sucrose concentration showed a significant effect on the degradation of the HCAs
365 (Figure 7b). Degradation increases smoothly with an increase in pH from 4.75 to 5.0
366 but decreases gradually when the pH exceeds 5.0, at any given concentration of
367 sucrose. The negative effect on total HCA degradation at lower pH than the optimal
368 may be attributed to the scavenging effect of H^+ or •OH radicals which can inhibit the
369 reduction of Fe(III) to Fe(II) and prevent the further generation of •OH radicals (*49,*
370 *50*). On the other hand, the negative effect at pH above the optimal may be
371 attributable to the deactivation of the Fe(II) catalyst with the formation of Fe(III)
372 oxyhydroxide *in lieu* of being regenerated back to Fe(II) (*51*). The formation of
373 Fe(III) oxyhydroxides in the present study was confirmed by analysing the
374 precipitates obtained at pH 5.5 and 25 °C, by XRD (Table 3). The *d*-spacing values
375 6.21 Å, 3.28 Å, 2.46 Å and 2.36 Å correspond to lepidocrocite (*i.e.*, iron(III) oxide
376 hydroxide), FeO(OH), while the peaks at 5.20 Å and 2.04 Å is associated with CaA
377 (*52*). The formation of oxyhydroxide is derived from the following reaction equation
378 (Eq. (7)):

$$Fe^{2+} + ¼O_2 + 2OH^- \rightarrow FeOOH + ½H_2O \quad (7)$$

379 Figure 7c shows the interaction effects of pH and temperature on HCA degradation.
380 The non-significance of the temperature variable is evident by the narrow range on
381 the response axis (*i.e.*, 57–64%). Despite this, the degradation trend on the HCAs in
382 terms of temperature is still observable. Increasing temperature leads to less
383 degradation of the HCAs. The decomposition of H_2O_2 by Fe(II) is not directly linked
384 to the amount of HCA degraded. In addition to the formation of •OH radicals by the
385 Fenton process, non-reactive species such as H_2O and O_2 are also formed at higher
386 temperatures (> 40 °C) (*53*). The Fenton process was the only contributor to the
387 degradation of HCAs as there was no thermal decomposition of any of the HCAs
388 within the temperature range studied (25–50 °C).

389 **Process optimization and model validation**

390 Numerical optimization was performed on the basis of the desirability function to
391 determine the optimum process parameters for the degradation of the HCAs. The
392 desirability function is expressed numerically from a scale of 0 to 1 (lowest to highest
393 desirability) and denotes the degree of importance in obtaining the desired response
394 value (*54*). A desirability function value can be constructed by using five different
395 goal optimization constraints: none, maximum, minimum, target and within range.
396 On the basis of the fitted quadratic models, an optimized response value can then be
397 predicted by using the chosen goal optimization criteria that maximizes the
398 desirability function. In order to simultaneously optimize numerous responses (*i.e.*,
399 multi-response optimization), the desirability function values for each response (*i.e.*,
400 CaA, *p*CoA and FeA) are combined into an overall desirability function by computing
401 their geometric mean of different desirability values, as shown in Eq.(8) (*55*).

$$D = (d_1 \times d_2 \times d_3 \times ... \times d_n)^{\frac{1}{n}} = \left(\prod_{i=1}^{n} d_1 \right)^{\frac{1}{n}} \quad (8)$$

where D is the overall desirability function, d_i is the desirability of the response and n is the number of responses investigated.

In order to confirm the accuracy and robustness of the predicted models and assess its reliability to predict the (%) degradation of HCAs, additional experiments were carried out under those conditions, as well as selected conditions of process streams close to that of a typical Australian sugar mill.

For this study, the desirability functions for the three individual HCA degradation models were combined into one value and compared to the desirability function of the total HCA model (Table 4). The combined desirability function values of the three individual HCA models for the experiments were relatively close to the desirability values produced for the single total HCA degradation model. This indicates that there is little variation between the simultaneously predicted values of each HCA degraded and the predicted value for the total HCA degraded.

Table 2 shows the experimental and predicted values (in parentheses) for the degradation of each and the total of the HCAs, under specified constraints. The optimum conditions for maximum degradation of HCAs (200 mg/L) using the Fenton process (2.49 mM $FeSO_4.7H_2O$ and 7.5 mM H_2O_2) are 0 mass% sucrose (*i.e.*, aqueous), pH 4.73 and 25.15 °C. Under these conditions 92% CaA, 69% *p*CoA and 70% FeA (total degradation of 77%) was degraded. The experimental values of the optimum conditions agree well with the predicted values deduced from each of the four models. The low error in the experimental and predicted values indicates good

423 agreement of the results. The experimental values obtained for the worst conditions
424 were also in good agreement with the predicted values. The good agreement between
425 values is attributable to the high combined desirability function value. It is worth
426 mentioning that the sum of the predicted degradation values of the individual HCA
427 degradation models (*i.e.*, CaA, *p*CoA and FeA) is not equal to the predicted total HCA
428 degradation values. Hence, the individual degradation models should be only used as
429 a guide to predict the degradation of the total HCAs present in a mixture.

430 The best results for the synthetic juices are obtained with solutions having similar
431 sucrose content and operating temperature as factory mixed juice (synthetic juice 1)
432 followed by factory No. 1 mill juice (*i.e.*, juice expressed from the first mill of a
433 quintuple set of mills) (synthetic juice 2). Despite a low desirability function value
434 predicted under the synthetic juice 1 conditions, the experimental results were in close
435 agreement with the predicted values for all four models. The lower desirability may
436 be due to some of the constraints that were not close to any of the design points of the
437 CCD. On the other hand, a higher error was observed for synthetic juice 2, despite a
438 reasonable desirability value. In addition, the experimental values obtained for *p*CoA
439 and FeA degradation were significantly lower than the predicted values. Then again,
440 the calculated total HCA degradation (76%) based on the predicted degradation
441 values of CaA (68%), *p*CoA (75%) and FeA (84%) degradation models is higher than
442 the model predicted total HCA degradation (67%). It is highly probable therefore,
443 that the presence of sucrose may have contributed to the inaccuracy of this prediction
444 as its concentration was outside the range used to develop the proposed models.
445 Therefore, it is not recommended to use constraints outside the ranges studied for
446 multi-response optimization, as the responses are all dependent on each other.

From these results, the Fenton process can successfully be used to degrade HCAs (*i.e.*, color precursor compounds) in a raw sugar manufacturing factory, as minimum sucrose breakdown occurred. However, the effectiveness of the Fenton process will be expected to be dependent on the type of sugarcane cultivar, the harvesting conditions, cane maturity, and location. This is also because the proportion and ratio of free and conjugated phenolics will influence degradation. Despite this, the Fenton process will be particularly useful in processing juice expressed from the whole sugar cane biomass (instead of the stalk) because of the prevalent of color precursors in such juice types. As the sugar cane industry around the world is looking towards diversification by value-adding with the excess biomass produced from whole crop processing, the use of the Fenton or similar processes will allow juice expressed from the whole sugarcane plant to be cost-effectively processed. The advantages of the use of the Fenton process in the sugar manufacturing process include its simplicity, its non-specific oxidation property and the use of inexpensive equipment. Also, the sludge that is produced has the potential to remove colorants and other impurities (including proteins and polysaccharides) improving the quality of the juice feedstock.

ACKNOWLEDGMENTS

The authors wish to thank Sugar Research Development and Corporation (Brisbane, Australia) and Sugar Research Limited (Brisbane, Australia) for financial assistance in the project. The authors also thank Mr. Tony Raftery of the IFE Central Analytical Research Facility at the Queensland University of Technology for his assistance in the XRD analyses.

Supporting Information

ANOVA for model terms of the response surface reduced quadratic models, Box-Cox plots of CaA, *p*CoA, FeA and total HCA degradation data for the determination of the optimized power transformed response surface model, and normal probability plots of residuals for fitted models using CaA, *p*CoA, FeA and total HCA degradation data after power transformation. This material is available free of charge via the Internet at http://pubs.acs.org.

REFERENCES

1. Ho, C. T., Phenolic compounds in food: an overview. In *Phenolic Compounds in Food and Their Effects on Health I: Analysis, Occuurence, and Chemistry*, Ho, C. T.; Lee, C. Y.; Huang, M. T., Eds. American Chemical Society: Washington, DC, 1992; Vol. 506, pp 2-7.

2. Lucas, M. S.; Peres, J. A.; Amor, C.; Prieto-Rodríguez, L.; Maldonado, M. I.; Malato, S., Tertiary treatment of pulp mill wastewater by solar photo-Fenton. *J. Hazard. Mater.* **2012,** *225–226*, 173-181.

3. Kuo, C. Y.; Pai, C. Y.; Wu, C. H.; Jian, M. Y., Effects of oxidant concentration and temperature on decolorization of azo dye: comparisons of UV/Fenton and UV/Fenton-like systems. *Water Sci. Technol.* **2012,** *65*, 1970-1974.

4. Wang, Y.; Li, X.; Zhen, L.; Zhang, H.; Zhang, Y.; Wang, C., Electro-Fenton treatment of concentrates generated in nanofiltration of biologically pretreated landfill leachate. *J. Hazard. Mater.* **2012,** *229–230*, 115-121.

5. Babuponnusami, A.; Muthukumar, K., Degradation of phenol in aqueous solution by Fenton, sono-Fenton and sono-photo-Fenton methods. *Clean: Soil, Air, Water* **2011,** *39*, 142-147.

493 6. Nichela, D.; Haddou, M.; Benoit-Marquié, F.; Maurette, M.-T.; Oliveros, E.;
494 García Einschlag, F. S., Degradation kinetics of hydroxy and hydroxynitro derivatives
495 of benzoic acid by fenton-like and photo-fenton techniques: A comparative study.
496 *Appl. Catal., B* **2010,** *98*, 171-179.
497 7. Li, Y.; Bachas, L. G.; Bhattacharyya, D., Selected chloro-organic
498 detoxifications by polychelate (poly(acrylic acid)) and citrate-based Fenton reaction at
499 neutral pH environment. *Ind. Eng. Chem. Res.* **2007,** *46*, 7984-7992.
500 8. Catrinescu, C.; Arsene, D.; Apopei, P.; Teodosiu, C., Degradation of 4-
501 chlorophenol from wastewater through heterogeneous Fenton and photo-Fenton
502 process, catalyzed by Al–Fe PILC. *Appl. Clay Sci.* **2012,** *58*, 96-101.
503 9. Segura, Y.; Martínez, F.; Melero, J. A.; Molina, R.; Chand, R.; Bremner, D. H.,
504 Enhancement of the advanced Fenton process (Fe^0/H_2O_2) by ultrasound for the
505 mineralization of phenol. *Appl. Catal., B* **2012,** *113–114*, 100-106.
506 10. Arsene, D.; Musteret, C. P.; Catrinescu, C.; Apopei, P.; Barjoveanu, G.;
507 Teodosiu, C., Combined oxidation and ultrafiltration processes for the removal of
508 priority organic pollutants from wastewaters. *Environ. Eng. Manag. J.* **2011,** *10*,
509 1967-1976.
510 11. Üstün, G. E.; Solmaz, S. K. A.; Birgül, A., Regeneration of industrial district
511 wastewater using a combination of Fenton process and ion exchange—A case study.
512 *Resour. Conserv. Recy.* **2007,** *52*, 425-440.
513 12. Elías-Maxil, J. A.; Rigas, F.; Orta De Velásquez, M. T.; Ramírez-Zamora, R.-
514 M., Optimization of Fenton's reagent coupled to dissolved air flotation to remove
515 cyanobacterial odorous metabolites and suspended solids from raw surface water.
516 *Water Sci. Technol.* **2011,** *64*, 1668-1674.

517 13. Khoddami, A.; Wilkes, M. A.; Roberts, T. H., Techniques for Analysis of
518 Plant Phenolic Compounds. *Molecules* **2013,** *18*, 2328-2375.
519 14. Herrmann, K., Occurrence and Content of Hydroxycinnamic and
520 Hydroxybenzoic Acid Compounds in Foods. *Crit Rev Food Sci* **1989,** *28*, 315-347.
521 15. Heredia, J. B. D.; Torregrosa, J.; Dominguez, J. R.; Peres, J. A., Kinetic model
522 for phenolic compound oxidation by Fenton's reagent. *Chemosphere* **2001,** *45*, 85-90.
523 16. Du, Y.; Zhou, M.; Lei, L., Role of the intermediates in the degradation of
524 phenolic compounds by Fenton-like process. *J. Hazard. Mater.* **2006,** *B136*, 859-865.
525 17. Amat, A. M.; Arques, A.; Beneyto, H.; García, A.; Miranda, M. A.; Seguí, S.,
526 Ozonisation coupled with biological degradation for treatment of phenolic pollutants:
527 a mechanistically based study. *Chemosphere* **2003,** *53*, 79-86.
528 18. Azabou, S.; Najjar, W.; Gargoubi, A.; Ghorbel, A.; Sayadi, S., Catalytic wet
529 peroxide photo-oxidation of phenolic olive oil mill wastewater contaminants Part II.
530 Degradation and detoxification of low-molecular mass phenolic compounds in model
531 and real effluent. *Appl. Catal., B* **2007,** *77*, 166-174.
532 19. Gernjak, W.; Krutzler, T.; Glaser, A.; Malato, S.; Caceres, J.; Bauer, R.;
533 Fernández-Alba, A. R., Photo-Fenton treatment of water containing natural phenolic
534 pollutants. *Chemosphere* **2003,** *50*, 71-78.
535 20. Kusvuran, E.; Samil, A.; Atanur, O. M.; Erbatur, O., Photocatalytic
536 degradation kinetics of di- and tri-substituted phenolic compounds in aqueous solution
537 by TiO_2/UV. *Appl. Catal., B* **2005,** *58*, 211-216.
538 21. Monteagudo, J. M.; Durán, A.; Aguirre, M.; San Martín, I., Optimization of
539 the mineralization of a mixture of phenolic pollutants under a ferrioxalate-induced
540 solar photo-Fenton process. *J. Hazard. Mater.* **2011,** *185*, 131-139.

22. Morelli, R.; Russo-Volpe, S.; Bruno, N.; Lo Scalzo, R., Fenton-dependent damage to carbohydrates: free radical scavenging activity of some simple sugars. *J. Agric. Food Chem.* **2003,** *51*, 7418-7425.

23. Nguyen, D. M. T.; Doherty, W. O. S., Phenolics in sugar cane juice: Potential degradation by hydrogen peroxide and Fenton's reagent. *Int Sugar J* **2012,** *114*, 309-315.

24. Paton, N. H., The origin of colour in raw sugar. *Proceedings of Australian Society of Sugar Cane Technologists* **1992**, 8-17.

25. Nguyen, D. M. T.; Doherty, W. O. S., Optimisation of process parameters for the removal of hydroxycinnamic acids in sugar solutions *Int Sugar J* **2013,** *1377*, 642-647.

26. Montgomery, D. C., *Design and Analysis of Experiments*. 7th ed.; John Wiley & Sons: New York, 2008.

27. Box, G. P. E.; Cox, D. R., An analysis of transformations. *J. Roy. Stat. Soc.* **1964,** *B26*, 211-243.

28. Morgan, B.; Lahav, O., The effect of pH on the kinetics of spontaneous Fe(II) oxidation by O_2 in aqueous solution – basic principles and a simple heuristic description. *Chemosphere* **2007,** *68*, 2080-2084.

29. Cornard, J.-P.; Caudron, A.; Merlin, J.-C., UV–visible and synchronous fluorescence spectroscopic investigations of the complexation of Al(III) with caffeic acid, in aqueous low acidic medium. *Polyhedron* **2006,** *25*, 2215-2222.

30. Hynes, M. J.; O'Coinceanainn, M., The kinetics and mechanisms of reactions of iron(III) with caffeic acid, chlorogenic acid, sinapic acid, ferulic acid and naringin. *J. Inorg. Biochem.* **2004,** *98*, 1457-1464.

565 31. Rivas, F. J.; Beltrán, F. J.; Garcia-araya, J. F.; Navarrete, V.; Gimeno, O., Co-
566 oxidation of *p*-hydroxybenzoic acid and atrazine by the Fenton's like system
567 Fe(III)/H_2O_2. *J. Hazard. Mater.* **2002,** *B91*, 143-157.
568 32. Adams, M. L.; O'Sullivan, B.; Downard, A. J.; Powell, K. J., Stability
569 constants for aluminum(III) complexes with the 1,2-dihydroxyaryl ligands caffeic
570 acid, chlorogenic acid, DHB, and DASA in aqueous solution. *J. Chem. Eng. Data*
571 **2002,** *47*, 289-296.
572 33. Sánchez-Cortés, S.; García-Ramos, J. V., Photoinduced coupling and
573 adsorption of caffeic acid on silver surface studied by surface-enhanced Raman
574 spectroscopy. *Spectrochim. Acta, Part A* **1999,** *55*, 2935-2941.
575 34. Dürüst, N.; Özden, S.; Umur, E.; Dürüst, Y.; Küçükislamoğlu, M., The
576 isolation of carboxylic acids from the flowers of *Delphinium formosum*. *Turk. J.*
577 *Chem.* **2001,** *25*, 93-97.
578 35. Machado, N. F. L.; Calheiros, R.; Gaspar, A.; Garrido, J.; Borges, F.; Marques,
579 M. P. M., Antioxidant phenolic esters with potential anticancer activity: Solution
580 equilibria studied by Raman spectroscopy. *J. Raman Spectrosc.* **2009,** *40*, 80-85.
581 36. Świsłocka, R., Spectroscopic (FT-IR, FT-Raman, UV absorption, ^{1}H and ^{13}C
582 NMR) and theoretical (in B3LYP/6-311++G** level) studies on alkali metal salts of
583 caffeic acid. *Spectrochim. Acta, Part A* **2012,** *in press*.
584 37. Świsłocka, R.; Kowczyk-Sadowy, M.; Kalinowska, M.; Lewandowski, W.,
585 Spectroscopic (FT-IR, FT-Raman, ^{1}H and ^{13}C NMR) and theoretical studies of *p*-
586 coumaric acid and alkali metal *p*-coumarates. *Spectrosc.-Int. J.* **2012,** *27*, 35-48.
587 38. Kalinowska, M.; Świsłocka, R.; Lewandowski, W., Zn(II), Cd(II) and Hg(I)
588 complexes of cinnamic acid: FT-IR, FT-Raman, ^{1}H and ^{13}C NMR studies. *J. Mol.*
589 *Struct.* **2011,** *993*, 404-409.

590 39. Hanna, K.; Quilès, F., Surface complexation of 2,5-dihydroxybenzoic acid
591 (gentisic acid) at the nanosized hematite−water interface: An ATR-FTIR study and
592 modeling approach. *Langmuir* **2011,** *27*, 2492-2500.
593 40. Dobson, K. D.; McQuillan, A. J., In situ infrared spectroscopic analysis of the
594 adsorption of aromatic carboxylic acids to TiO_2, ZrO_2, Al_2O_3, and Ta_2O_5 from
595 aqueous solutions. *Spectrochim. Acta, Part A* **2000,** *56*, 557-565.
596 41. Vasko, P. D.; Blackwell, J.; Koenig, J. L., Infrared and raman spectroscopy of
597 carbohydrates: Part I: Identification of O–H and C–H-related vibrational modes for D-
598 glucose, maltose, cellobiose, and dextran by deuterium-substitution methods.
599 *Carbohydr. Res.* **1971,** *19*, 297-310.
600 42. Huvenne, J. P.; Vergoten, G.; Fleury, G.; Legrand, P., Champ de forces de
601 symetrie locale de molecules cycliques: III. Interprétation des spectres de vibration du
602 glucose cristallisé sous les deux formes α et β. *J. Mol. Struct.* **1981,** *74*, 169-180.
603 43. Kodad, H.; Mokhlisse, R.; Davin, E.; Mille, G., Étude IRTF par réflexion
604 totale atténuée (ATR) de sucres en solution aqueuse. *Can. J. Appl. Spectrosc.* **1994,**
605 *39*, 107-112.
606 44. Kačuráková, M.; Mathlouthi, M., FTIR and laser-Raman spectra of
607 oligosaccharides in water: characterization of the glycosidic bond. *Carbohydr. Res.*
608 **1996,** *284*, 145-157.
609 45. Max, J.-J.; Chapados, C., Sucrose hydrates in aqueous solution by IR
610 spectroscopy. *Journal of Physical Chemistry A* **2001,** *105*, 10681-10688.
611 46. Varsányi, G., *Assignments for Vibrational Spectra of Seven Hundred Benzene*
612 *Derivatives*. Adam Hilger: London, 1974; Vol. 1.

613 47. Yost, E. C.; Tejedor-Tejedor, M. I.; Anderson, M. A., In situ CIR-FTIR
614 characterization of salicylate complexes at the goethite/aqueous solution interface.
615 *Environ. Sci. Technol.* **1990,** *24*, 822-828.
616 48. Gilfillan, W. N.; Nguyen, D. M. T.; Sopade, P. A.; Doherty, W. O. S.,
617 Preparation and characterisation of composites from starch and sugar cane fibre. *Ind.*
618 *Crop. Prod.* **2012,** *40*, 45-54.
619 49. Rivas, F. J.; Frades, J.; Alonso, M. A.; Montoya, C.; Monteagudo, J. M.,
620 Fenton's oxidation of food processing wastewater components. Kinetic modeling of
621 protocatechuic acid degradation. *J. Agric. Food Chem.* **2005,** *53*, 10097-10104.
622 50. Deng, Y., Physical and oxidative removal of organics during Fenton treatment
623 of mature municipal landfill leachate. *J. Hazard. Mater.* **2007,** *146*, 334-340.
624 51. Bigda, R. J., Consider Fenton's chemistry for Fenton wastewater treatment.
625 *Chem. Eng. Prog.* **1995,** *91*, 62-66.
626 52. Dong, W.; Xu, Y.; Ren, J.; Chu, H.; Li, J.; Liu, X.; Chen, M., Synthesis and
627 characterization of biodegradable polymers composed of 3,4-dihydroxycinnamic acid
628 and poly(ethylene glycol). *J. Appl. Polym. Sci.* **2012,** *125*, 1657-1662.
629 53. Rodrigues, C. S. D.; Madeira, L. M.; Boaventura, R. A. R., Treatment of
630 textile effluent by chemical (Fenton's Reagent) and biological (sequencing batch
631 reactor) oxidation. *J. Hazard. Mater.* **2009,** *172*, 1551-1559.
632 54. Harrington, E. C., The desirability function. *Ind. Qual. Control* **1965,** *21*, 494-
633 498.
634 55. Derringer, G.; Suich, R., Simultaneous optimization of several response
635 variables. *J. Qual. Technol.* **1980,** *12*, 214-219.
636
637

Tables and Figures

Tables

Table 1 Coded and Actual Values of the Experimental Design.

Table 2 Wavenumbers (cm^{-1}) ofSselected bands from ATR-FTIR Spectra of CaA solution and CaA Mixtures containing Fe(II) and/or Sucrose at pH 5.5.

Table 3 XRD Data of the Precipitate Formed between CaA and Fe(II) at pH 5.5 and 25 °C.

Table 4 Optimized Conditions under Specified Constraints for the Degradation of Total HCA (200 mg/L) and Model Verification.

Figures

Figure 1 Normal probability plot of residuals for fitted model using CaA degradation data before power transformation.

Figure 2 Plot of predicted response and experimental (actual) values for the degradation (%) of (a) CaA; (b) *p*CoA; (c) FeA; and (d) total HCA.

Figure 3 Perturbation plot for the degradation (%) of (a) CaA; (b) *p*CoA; and (c) FeA. Coded values are shown for each factor: total HCA (*A*); sucrose (*B*); pH (*C*); and temperature (*D*); and refer to actual values listed in Table 1.

Figure 4 Effect of pH (4.0-6.0) on the absorption spectra of CaA (0.055 mM): (a) in the absence and (b) in the presence of Fe(II) (0.04 mM).

Figure 5 Normalized ATR-FTIR spectra of CaA solutions after subtraction of acetate buffer (pH 5.5): (a) in the absence and (b) in the presence of Fe(II).

Figure 6 Normalized ATR-FTIR spectra of CaA solutions containing sucrose after subtraction of acetate buffer (pH 5.5): (a) in the absence and (b) in the presence of Fe(II).

Figure 7 Three-dimensional surface plots of total HCA degradation (%) as a function: (a) total HCA and sucrose; (b) sucrose and pH; and (c) pH and temperature (bottom). Variables: Total HCA (155 mg/L); sucrose (7.5 mass%); pH (5.0) and temperature (35 °C).

Table 1

Notation	Factor	Unit	Coded Levels of Parameters				
			–2	**–1**	**0**	**+1**	**+2**
A (X_1)	Total HCA	mg/L	20	65	110	155	200
B (X_2)	Sucrose	mass%	0	3.75	7.50	11.25	15
C (X_3)	pH		4.5	4.75	5.0	5.25	5.5
D (X_4)	Temperature	°C	25	31.25	37.5	43.75	50

Table 2

CaA	CaA mixtures			Band Assignments*	
	Fe(II)	Fe(II) and sucrose	Sucrose		
		3401	3495	ν(OH)	
3274	3247			$\nu(OH)_{ar}$	
		3182	3113	ν(OH)	
2981	2981	2980	2980	$\nu(CH)_{C=C} + \nu(CH)$	
2921		2933	2933	ν(CH)	20a
		2900	2900	ν(CH)	
2854	2852			ν(OH)	
1672	1672	1669	1674	ν(C=O)	
1618	1608	1611	1619	$\nu(CC)_{C=C}$	
1554	1550	1567	1578	$\nu(CC)_{ar}$	8a
1524	1524			$\nu(CC)_{ar}$	8b
1483	1483			$\nu(CC)_{ar}$	19a
1454	1454	1454	1454	$\nu(CC)_{ar}$	19b
		1426	1426	β(COH)	
1386	1388	1377	1377	$\nu(CC) + \beta(OH)_{ar}$	14
1328	1329	1332	1332	$\beta(CH)_{C=C}$	

1275	1265	1274	1266	ν(C–OH)	
		1210	1210	β(CH)	
1160	1160			β(CH)	18a
1118	1118			β(CH)	18b
1085	1085			β(OH)	
1045	1045	1045	1045	$\gamma(CH)_{C=C} + \gamma$(CH)	17b
		1018	1018	ν(C–O)	
		998	998	β(COH)	
		927	927	ν(CC)	
877	877	876	876		
		830	830	β(CCH)	

*Symbols are denoted as follows: ν (stretching vibrations); β (in-plane bending modes); γ (out-of-plane bending modes).

Table 3

Intensity (counts)	*d*-spacing (Å)	
	Precipitate	**FeO(OH)***
126.31	6.2164	6.2580
80.550	5.2003	
204.48	3.2821	3.2933
161.52	2.4644	2.4737
138.89	2.3609	2.3635
543.59	2.0409	
78.600	1.9320	1.9365
36.960	1.7282	1.7350
28.340	1.5252	1.5360
112.57	1.2941	1.2990

*Based on a FeO(OH) reference pattern from the International Centre for Diffraction Data (ICDD PDF card 04-010-4300).

Table 4

Experiment	Sucrose (mass%)	pH	T (°C)	% Degradation*				Desirability	
				CaA	*p*CoA	FeA	Total HCA	Combined	Total HCA
Water	0	4.73	25.15	92 (90)	69 (68)	70 (64)	77 (73)	0.720	0.743
Worst case	14.47	4.52	39.68	87 (90)	33 (37)	40 (46)	53 (49)	0.542	0.632
Synthetic Juice 1	13.00	5.39	35.98	73 (72)	48 (52)	51 (56)	57 (58)	0.383	0.332
Synthetic Juice 2	21.00	4.86	29.97	78 (68)	52 (75)	54 (84)	61 (67)	0.655	0.621

*Values in parentheses indicate model predicted % degradation of each individual/total HCA. Measurements were conducted in triplicate. RSD was < 5.0%.

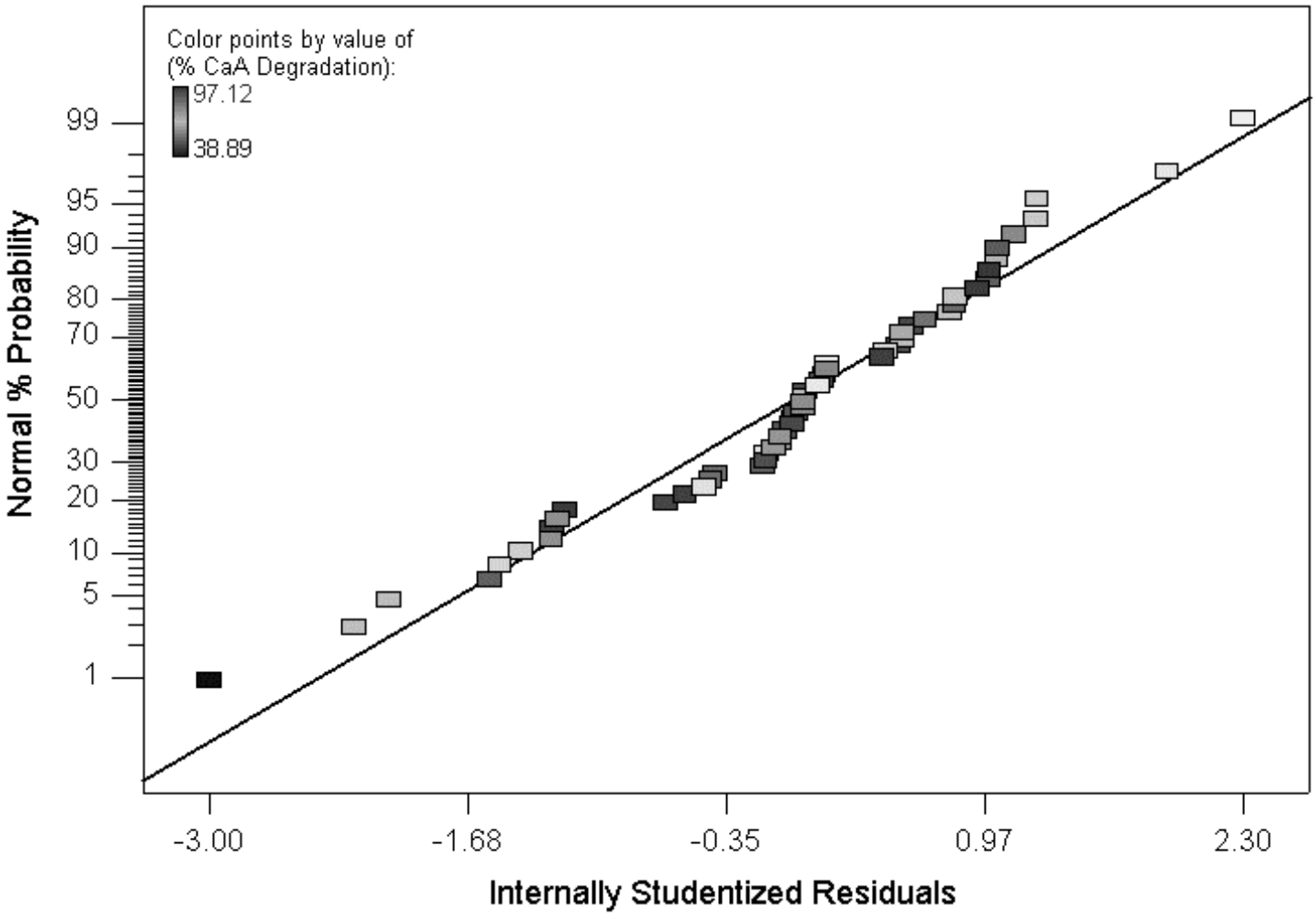
Color points by value of
(% CaA Degradation):
97.12
38.89
Normal % Probability
99
95
90
80
70
50
30
20
10
5
1
-3.00
-1.68
-0.35
0.97
2.30
Internally Studentized Residuals

Figure 1

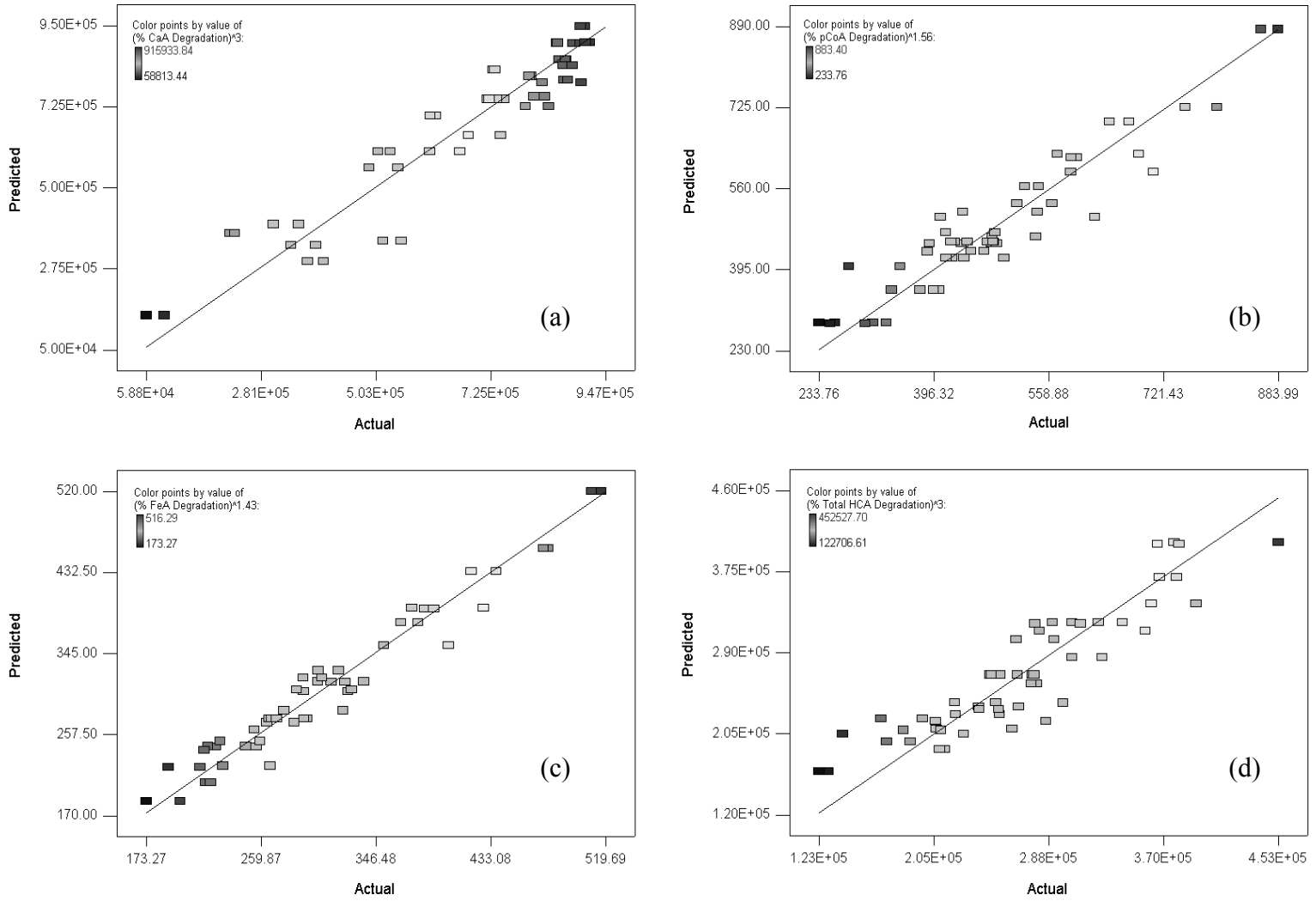
Color points by value of
(% CaA Degradation)^3:
915933.84
58813.44
Predicted
Actual
9.50E+05
7.25E+05
5.00E+05
2.75E+05
5.00E+04
5.88E+04
2.81E+05
5.03E+05
7.25E+05
9.47E+05
(a)
Color points by value of
(% pCoA Degradation)^1.56:
883.40
233.76
890.00
725.00
560.00
395.00
230.00
233.76
396.32
558.88
721.43
883.99
(b)
Color points by value of
(% FeA Degradation)^1.43:
516.29
173.27
520.00
432.50
345.00
257.50
170.00
173.27
259.87
346.48
433.08
519.69
(c)
Color points by value of
(% Total HCA Degradation)^3:
452527.70
122706.61
4.60E+05
3.75E+05
2.90E+05
2.05E+05
1.20E+05
1.23E+05
2.05E+05
2.88E+05
3.70E+05
4.53E+05
(d)

Figure 2

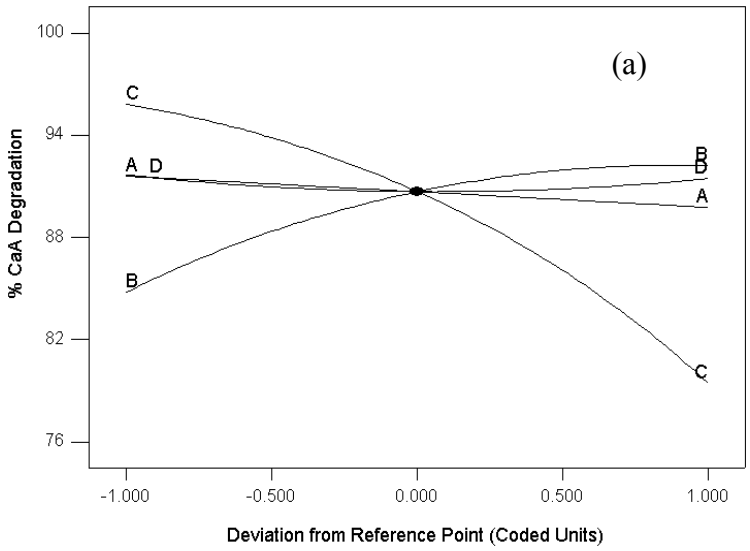
(a)
100
94
88
82
76
% CaA Degradation
C
A D
B
B
D
A
C
-1.000
-0.500
0.000
0.500
1.000
Deviation from Reference Point (Coded Units)

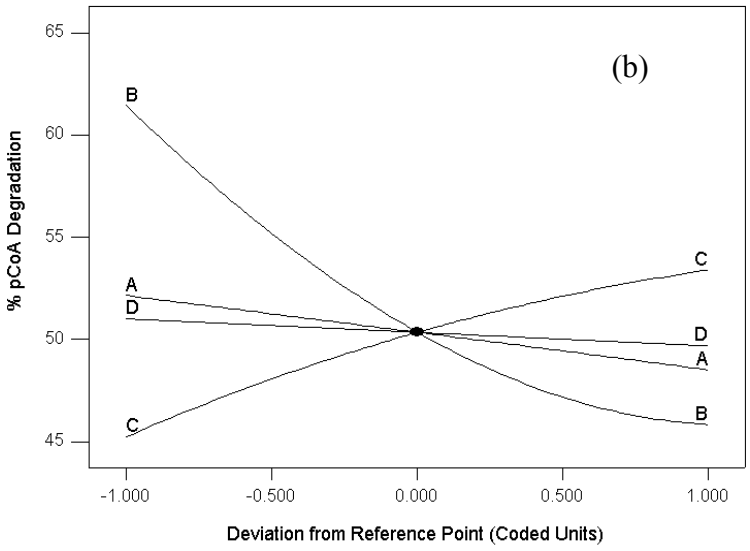
(b)
65
60
55
50
45
% pCoA Degradation
B
A
D
C
C
D
A
B
-1.000
-0.500
0.000
0.500
1.000
Deviation from Reference Point (Coded Units)

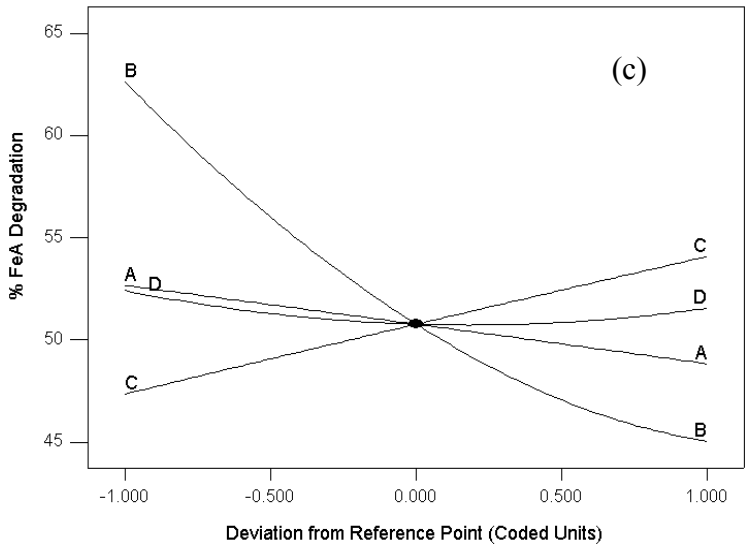
(c)
65
60
55
50
45
% FeA Degradation
B
A D
C
C
D
A
B
-1.000
-0.500
0.000
0.500
1.000
Deviation from Reference Point (Coded Units)

Figure 3

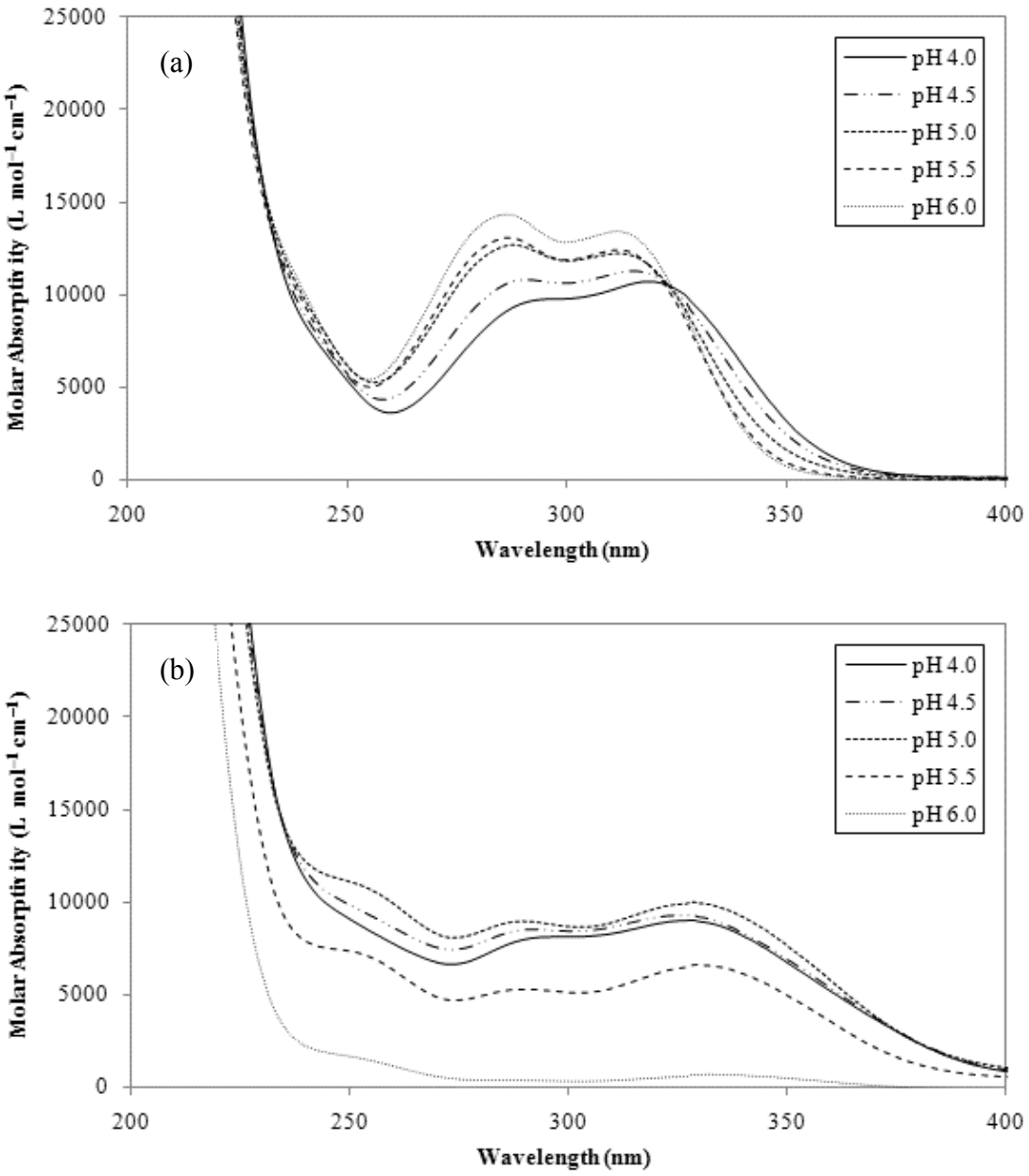
(a)
pH 4.0
pH 4.5
pH 5.0
pH 5.5
pH 6.0
Molar Absorptivity (L mol⁻¹ cm⁻¹)
Wavelength (nm)
(b)
pH 4.0
pH 4.5
pH 5.0
pH 5.5
pH 6.0
Molar Absorptivity (L mol⁻¹ cm⁻¹)
Wavelength (nm)

Figure 4

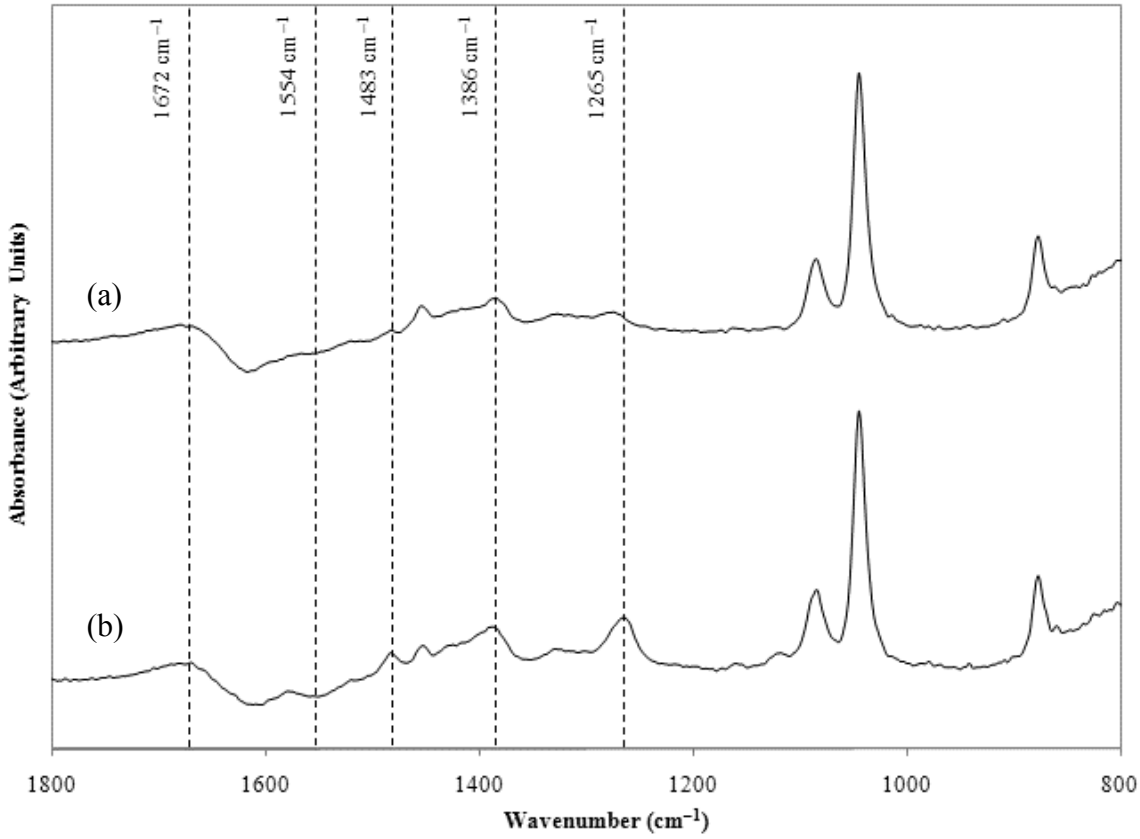
1672 cm⁻¹
1554 cm⁻¹
1483 cm⁻¹
1386 cm⁻¹
1265 cm⁻¹
(a)
(b)
Absorbance (Arbitrary Units)
1800
1600
1400
1200
1000
800
Wavenumber (cm⁻¹)

Figure 5

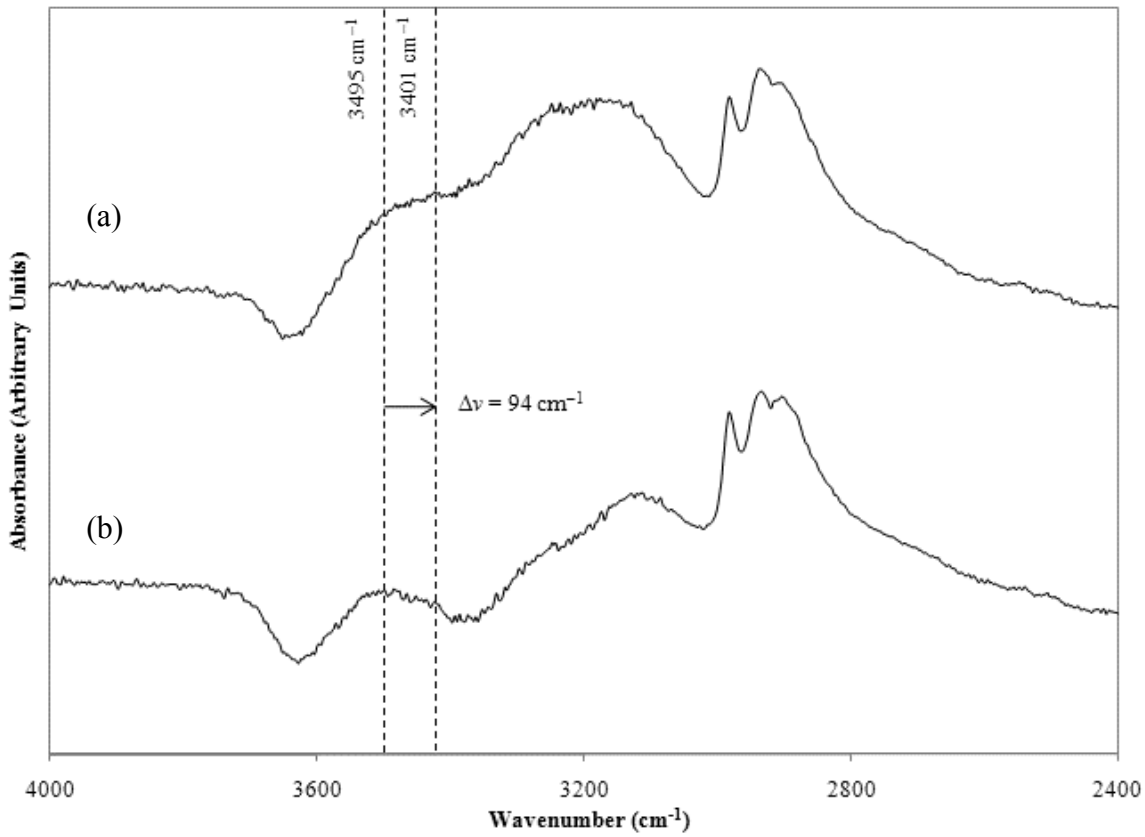
3495 cm⁻¹
3401 cm⁻¹
(a)
Δν = 94 cm⁻¹
(b)
Absorbance (Arbitrary Units)
4000
3600
3200
2800
2400
Wavenumber (cm⁻¹)

Figure 6

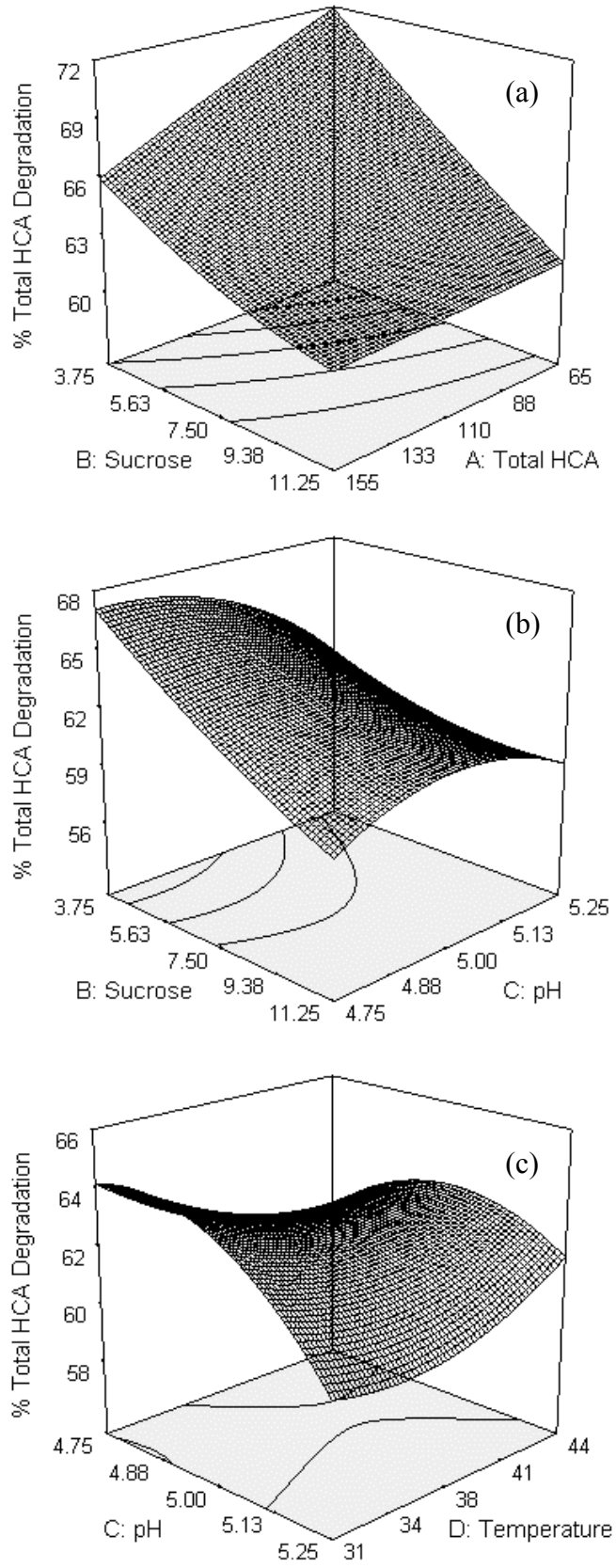
(a)
% Total HCA Degradation
72
69
66
63
60
3.75
5.63
7.50
9.38
11.25
B: Sucrose
65
88
110
133
155
A: Total HCA
(b)
% Total HCA Degradation
68
65
62
59
56
3.75
5.63
7.50
9.38
11.25
B: Sucrose
5.25
5.13
5.00
4.88
4.75
C: pH
(c)
% Total HCA Degradation
66
64
62
60
58
4.75
4.88
5.00
5.13
5.25
C: pH
44
41
38
34
31
D: Temperature

Figure 7

TOC Graphic

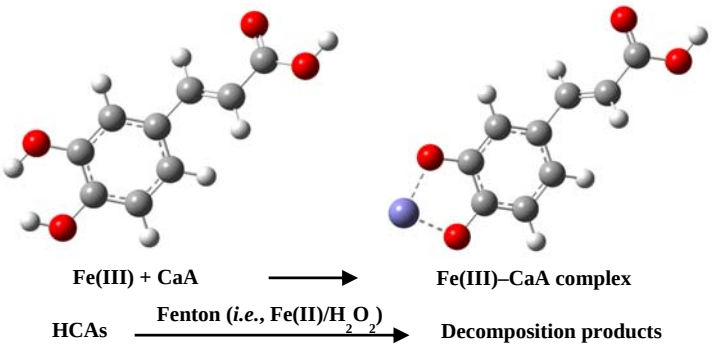
Fe(III) + CaA
Fe(III)–CaA complex
HCAs
Fenton (*i.e.*, Fe(II)/H2O2)
Decomposition products